A bestiary of genetic mouse lines and related tools for inducible and reversible intersectional misexpression

Elham Ahmadzadeh[1¶], Aditi Singh[1¶], N. Sumru Bayin[2], Xinli Qu[1], Linda Madisen[3], Daniel Stephen[2], Hongkui Zeng[3], Alexandra L. Joyner[2]* and Alberto Rosello-Diez[1]*

[1] *Australian Regenerative Medicine Institute, Monash University. Clayton, VIC 3800. Australia.*

[2] *Developmental Biology Program. Sloan Kettering Institute. New York, NY 10065. USA.*

[3] *Allen Institute for Brain Science. Seattle, WA 98109. USA*

¶ Equal contribution

***Correspondence:** alberto.rosellodiez@monash.edu (Twitter: @RoselloDiez); joynera@mskcc.org

Lead author: alberto.rosellodiez@monash.edu

Summary (150 words)

Thanks to the astonishing advances in genetic manipulation, mouse models have become very powerful in their ability to interrogate biological processes. Among functional experiments, misexpression approaches are often modular, such that distinct combinations of driver and effector lines can be used to achieve different effects. However, existing combinations have pitfalls that hinder sophisticated applications like tissue-specific reversible gain-of-function. Here, we put forward an approach that can leverage existing driver modules to achieve inducible and reversible transgene misexpression with high spatiotemporal resolution, by using an effector allele that requires the intersection of two drivers, Cre and (r)tTA. We present the mouse lines generated for such an approach, as well as proof-of-principle experiments using different organs. We also show that the approach can be extended to other animal models, using chicken embryos. These new tools will facilitate unraveling biological questions that were previously impeded by technical limitations, in multiple fields and organisms.

Keywords

Cre, (r)tTA, intersectional genetics, inducible and reversible gene misexpression, tissue-specific, Tigre locus, DRAGON allele, p21, Ccn2/Ctgf, diphtheria toxin, DTA, tox176.

INTRODUCTION

The wealth of genetic tools that have been developed for mouse to study biological questions *in vivo* have enabled extremely sophisticated experiments to be conducted. Especially useful is the modular nature of some tools, in which a mouse line expressing a protein that can induce gene expression if the right genetic elements are present (driver module) is crossed with a line carrying the genetic elements that respond to the driver molecule (effector module). In this way only the offspring combining both modules will show a specific change in gene expression (Kaczmarczyk and Jackson, 2015; Rosen et al., 2015). In particular, the Cre/loxP system is a very powerful method for temporal and spatial control of gene expression, by utilizing gene promoters or loci with specific expression patterns (Smedley et al., 2011). The system has recently reached an unprecedented degree of sophistication, for example by using knock-ins at a docking site 5' of *Hprt* for rapid development of numerous Cre-driver strains, and the use of different types of promoters to either capture endogenous expression or restrict it to very specific cell types (Korecki et al., 2019). Nevertheless, the Cre/loxP system is not devoid of pitfalls. First, although there are inducible versions of Cre (Feil et al., 2009), allowing for temporal control of its activation, the genomic modification induced by Cre is permanent. Hence, if the desired effect is dependent only on Cre activity, it cannot be reversed, hampering the possibility of studying the recovery process after the genetic manipulation. Moreover, despite the supposed specificity of the regulatory regions or loci used to drive Cre expression, it has been shown that most if not all of the so-called tissue-specific Cre lines are not exclusively expressed in the tissue of interest (Heffner et al., 2012), giving rise to off-target effects that can lead to misleading conclusions about the biological process being interrogated.

The possibility of reversibility has been addressed by using a different driver-effector combination, known as the Tet system, based on the tetracycline (Tet) resistance operon of *E. coli* (Hillen and Berens, 1994). In the first version of this system, a transactivator fusion protein composed of the tetracycline repressor (tetR) and the activating domain of the herpes simplex viral protein 16 (VP16) can regulate the expression of a gene of interest using a Tet-responsive element (TRE) containing tet-operator (tetO) sequences. This system is known as Tet-Off, because in the presence of tetracycline or its analog doxycycline (Dox), the affinity of tetR to *tetO* sequences diminishes by 9 orders of magnitude, so that expression of the gene of interest is greatly reduced (Gossen and Bujard, 1992; St-Onge et al., 1996). Conversely, the Tet-On system is based on a reverse tetracycline-controlled transactivator (*rtTA*) derived from tTA through four amino acid changes in the tetR DNA binding moiety. This alters the binding properties of rtTA such that it can only recognize the *tetO* sequences in the presence of Dox (Gossen et al., 1995). While the first

generation tool was quite leaky, showing expression in the absence of Dox, subsequent mutations improved the sensitivity and specificity of rtTA, rendering it a useful tool (Urlinger et al., 2000). Another problem that initially encumbered Tet systems was that the TRE DNA sequences can be inactivated through epigenetic mechanisms, rendering them unreliable unless de-repressed by additional genetic modules (Godecke et al., 2017). Fortunately, this drawback was overcome when a systematic screen identified a locus in the mouse genome that does not show this inactivation (Zeng et al., 2008). Indeed, *Tigre* (also known as *Igs7*) is an intergenic region on mouse chromosome 9 that provides a safe harbor from which TRE-dependent expression can be tightly regulated (hence the name).

Despite these advances, however, both the Cre/loxP and the Tet-On/Off systems are still prone to off-target effects due to non-specificity of the promoter sequences or gene loci driving the expression of Cre/(r)tTA. One way to address this caveat is to employ separate fragments of the Cre recombinase (known as "split cre") that are expressed from distinct drivers, resulting in Cre activity (loxP excision) only in the intersectional cell population where both halves of Cre are expressed (Hirrlinger et al., 2009). A similar intersectional approach is to have a responder module that depends on two types of recombinases (e.g. Cre and Flp), such as the systems developed by the Dymecki lab (Dymecki and Kim, 2007). However, both approaches are still encumbered by the irreversibility problem.

The only strategy so far that addresses both the off-target and irreversibility problems has been developed by our labs (Madisen et al., 2015; Rosello-Diez et al., 2018). It involves combining the Cre/loxP and Tet systems such that the *Tigre* locus is targeted with a double conditional allele in which expression of the gene of interest (GOI) depends both on previous exposure to Cre (to prime the system through elimination of a STOP sequence upstream of the GOI) and on (r)tTA activity (through a TRE upstream of the floxed-STOP-GOI cassette). The first version of this system that includes a tdTomato (tdT) coding sequence within the floxed cassette was called DRAGON (Fig. 1A), standing for Doxycycline-dependent and Recombinase-Activated Gene OverexpressioN (Rosello-Diez et al., 2018). A *Dragon-p21* line was generated and used to study the cellular compensation mechanisms in the developing bones of the limbs when the cell cycle was blocked by transient p21 expression (Rosello-Diez et al., 2018). Since the DRAGON approach is intersectional, it is possible to achieve remarkable tissue-specificity (Fig. 1A), enabling the study of tissue-type dependent effects of gene misexpression. In addition, due to its dependence on (r)tTA, the system is inducible and reversible, allowing the effect of different times and durations of misexpression to be tested. Finally, by using different modules with particular GOIs to achieve similar outcomes (e.g. to reduce cell numbers by either blocking proliferation or inducing cell death), the system enables studies of how the type of insult influences biological responses.

Here we describe a series of new *Dragon* lines we have created (Fig. 1B) and provide a proof-of-principle for the kind of uses that they enable. We also provide an in-depth characterization of potential uses, including non-intersectional applications. We have focused most of our manipulations on two organs in developing mice: the limbs (and the bones within them) and the cerebellum. Growth of the long bones is driven by a cartilage template that is progressively replaced by bone (Kronenberg, 2003; Rosello-Diez and Joyner, 2015). In order to target the cartilage template, we used *Col2a1*-driven (r)tTA lines (Posey et al., 2009; Rosello-Diez et al., 2018). In order to restrict expression to the limb cartilage, we used a *Pitx2-Cre* allele (Shiratori et al., 2006) that drives Cre expression in the left lateral plate mesoderm (precursor of the left limb mesenchyme) at embryonic day (E) 8.5, with the right limb cartilage serving as an internal control (expressing only tdTomato). In the developing cerebellum, we targeted the cell lineage that generates the excitatory neurons using *Atoh1-Cre* (Matei et al., 2005) and *Atoh1-tTA* (Willett et al., in revision) lines. We also demonstrate that the approach can be applied in other *in vivo* systems using chicken embryos and co-electroporating the components. Given the wealth of Cre and (r)tTA tools already available, the constructs and mouse lines described here constitute a valuable resource for the scientific community, which will enable a wide variety of biological processes to be probed with unprecedented depth.

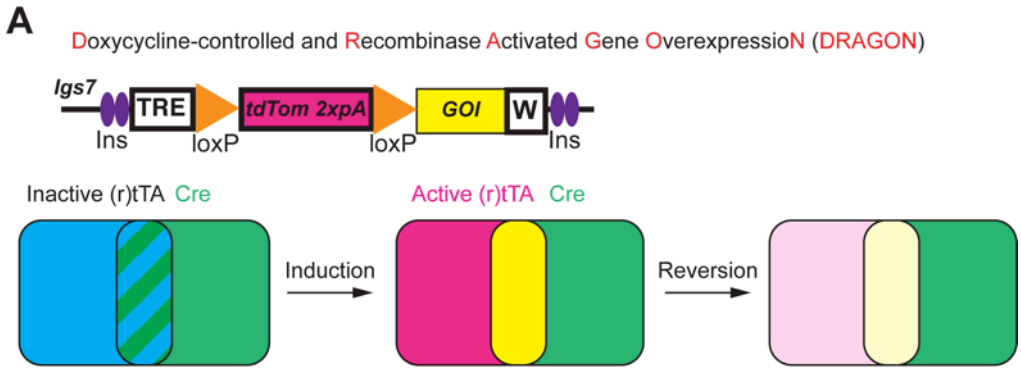

B

Available DRAGON mouse lines

Gene of interest	Use	Described in
Cdkn1a (*p21*)	Block proliferation	Rosello-Diez et al. 2018
Ctgf (*Ccn2*)	Signal imbalance	This manuscript
DTA (Diphtheria toxin)	Cell ablation	This manuscript

Figure 1. An intersectional genetic system for inducible and reversible gene misexpression. A) Schematic of the approach. Ins: insulators. W: Woodchuck virus RNA stabilizing sequence (WPRE). Expression of the Gene of interest (GOI) depends on both Cre and (r)tTA. In the presence of just Cre (green color), the floxed tdTomato-STOP cassette is eliminated, priming the system and deleting tdTomato (tdT), but the GOI is not expressed. In the presence of just (r)tTA (blue color), only the tdT embedded in the intact floxed cassette is expressed upon induction with(out) Doxycycline (pink color). It is only in the presence of both Cre and (r)tTA (hatched blue and green) that the GOI is expressed upon induction with(out) Doxycycline (yellow color). As the expression of both tdT and the GOI depends on (r)tTA activity, their expression is inducible and reversible,

and controlled by the addition/removal of Doxycycline. Lighter colors denote that the transgene expression is shut down. B) Table summarizing the available *Dragon* lines and their potential uses.

RESULTS AND DISCUSSION

A *Dragon-DTA* model can be used to generate acute tissue-specific cell ablation.

A common theme in developmental and regenerative biology is that different responses are elicited by cell ablation compared to defective cell proliferation. Therefore, to complement our *Dragon-p21* line, we generated an intersectional *Dragon-DTA* model (see Methods) to enable cell ablation with remarkable tissue specificity and temporal control, via expression of attenuated diphtheria toxin fragment A. We then combined it with mice bearing *Atoh1-tTA* (Willett et al. 2019, in revision) and *Atoh1-Cre* (Matei et al., 2005) to target the excitatory cerebellar nuclei (eCN), which house the main output neurons of the cerebellum (*eCN-DTA* model). Since the precursors of the cerebellar granule cells also express *Atoh1*, but starting only after E13.5 (Machold and Fishell, 2005) , we provided Dox at E13.5 to shut down tTA activity in them, restricting DTA expression to the eCN. As shown in Fig. 2A-D, this led to ectopic cell death (marked by TUNEL staining) specifically in the Nuclear Transitory Zone (NTZ), where the precursors of the eCN migrate from the rhombic lip. At P1, the number of eCN, revealed by MEIS2 immunostaining, was greatly reduced in *eCN-DTA* cerebella as compared to the controls (Fig. 2E-G). By choosing between the available *Cre* and *(r)tTA* lines, the *Dragon-DTA* strain will be a valuable resource to ablate cells with high spatiotemporal precision.

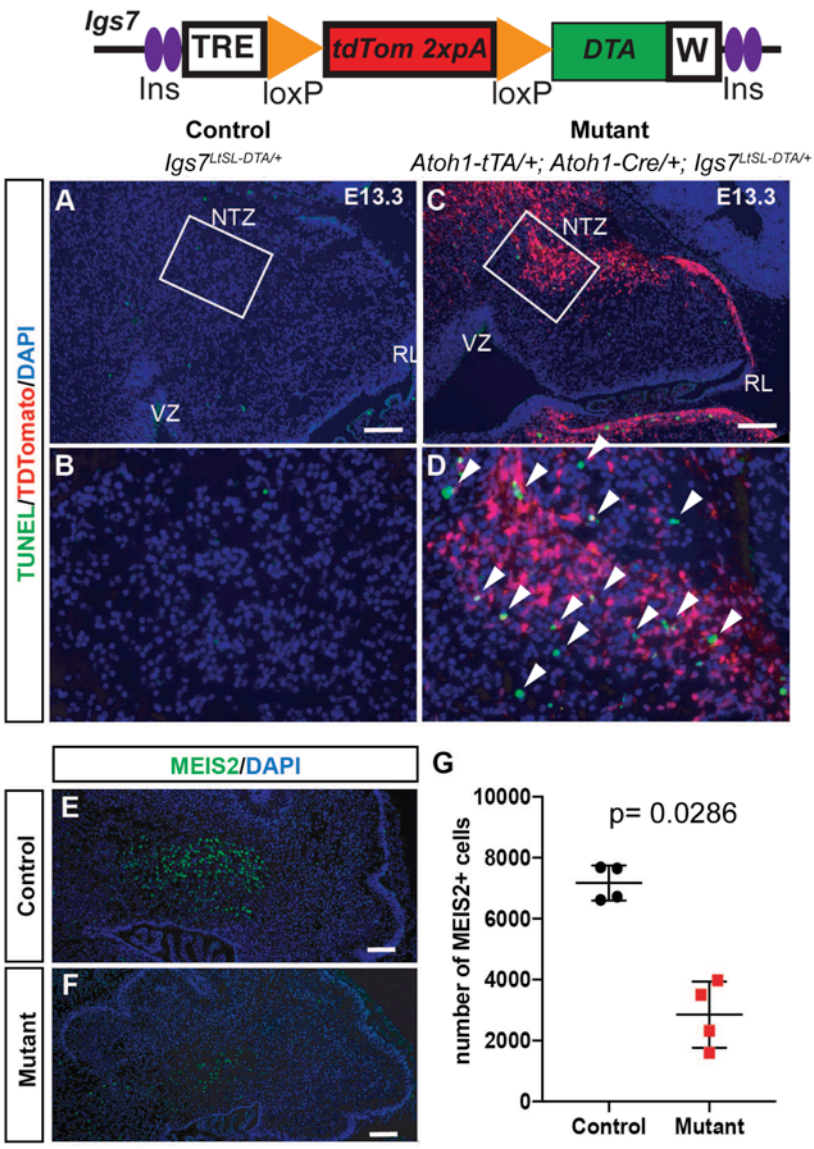

Figure 2. A *Dragon-DTA* model to generate acute tissue-specific cell ablation. A-D) Representative sagittal sections showing the cerebellar anlagen at E13.3 in *Dragon-DTA/+* embryos (control, n=4) and *eCN-DTA* embryos (experimental, n=3), in the absence of Dox. The boxed areas in (A, C) are shown magnified in (B, D). NTZ, nuclear transitory zone; VZ, ventricular zone; RL, rhombic lip. Arrowheads point to apoptotic cells (TUNEL$^+$). (E-G) Sagittal sections of cerebellar anlagen at P1, showing reduced numbers of MEIS2$^+$ cerebellar nuclei in *eCN-DTA* animals as compared to controls (n=4 for both). p-value for Mann-Whitney unpaired test is shown. Scale bars = 100 µm.

Unilateral misexpression of Connective Tissue Growth Factor in the growing skeletal elements leads to bone asymmetry.

We next searched for a versatile tool that could be used to transiently manipulate a variety of biological processes, such as development, homeostasis and repair. We reasoned that a molecule capable of interacting with several of the most commonly used signaling pathways would be an ideal candidate. Connective tissue growth factor (CTGF) has been described to exert such a pleiotropic effect (Takigawa, 2013). We thus generated a *Dragon-Ctgf* mouse model (see Methods) and combined it with mice bearing *Pitx2-Cre* and *Col2a1-tTA* (Tet-Off) drivers to achieve unilateral

expression of CTGF in the cartilage of the left limbs (*Pit-tTA-Ctgf* model, Fig. 3A). By postnatal day (P) 0-1, whereas the expression of *Ctgf* in the distal cartilage of the right *Pit-tTA-Ctgf* radius was very similar to the expression in WT animals (Fig. 3B-C), the expression in the left *Pit-tTA-Ctgf* element was more widespread (Fig. 3C). Interestingly, the ectopic expression of CTGF led to reduced growth of the left bones as early as embryonic day (E) 17.5, including deformation of the radius and ulna at postnatal stages (Fig. 3D). Given the strong effects we see, we expect the *Dragon-Ctgf* mouse line to become a valuable tool to study diverse processes such as growth, regeneration, fibrosis, etc.

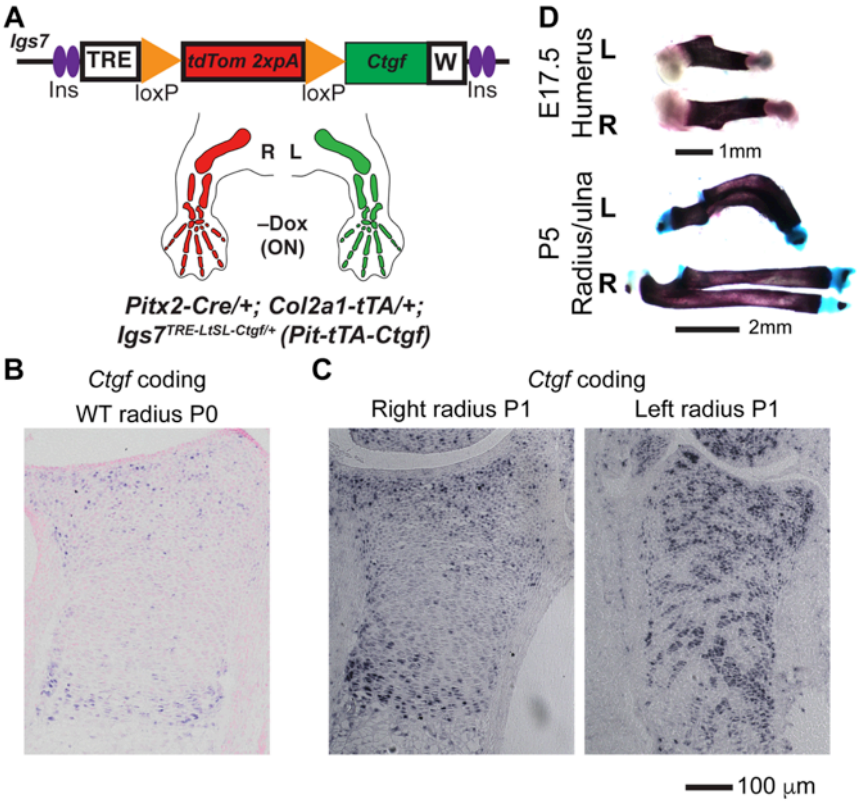

Figure 3. Unilateral overexpression of connective tissue growth factor leads to bone asymmetry. A) *Pit-tTA-Ctgf* model to achieve misexpression of *Ctgf* in the cartilage of the left limb. Note that *Col2a1-tTA* is used in this model, such that it is active by default and inactivated by Dox treatment (Tet-Off system). B, C) *In situ* hybridization for *Ctgf* mRNA in the distal radius cartilage from WT (B) and *Pit-tTA-Ctgf* mice (C) at P0-P1 (n=3). D) Representative examples of skeletal preparations of left and right *Pit-tTA-Ctgf* bones at the indicated stages (n=7 at E15.5, 2 at E17.5, 4 at P1, 1 at P5).

A model for reversible Connective Tissue Growth Factor misexpression in the growing skeletal elements reveals different outcomes of transient vs. permanent expression.

Besides its intersectional quality, a key aspect of the *Dragon* system is its reversibility. As a proof-of-principle for testing this application, we repeated the *Pit-tTA-Ctgf* experiment and supplied Dox to shut down tTA expression at E17.5 (Fig. 4A), when the phenotype is already obvious (Fig. 3D). As expected, *Ctgf* ceased to be overexpressed in the cartilage by P0-P1 (Fig. 4B). Moreover, when

the extent of asymmetry was compared with either continuous expression or transient overexpression, we found that the latter led to a much milder asymmetry than the former (Fig. 4C). The transient expression experiment thus suggests that there is a catch-up mechanism that allows limb growth to recover, and that would not have been discovered by irreversible misexpression, highlighting the utility of the new mouse lines.

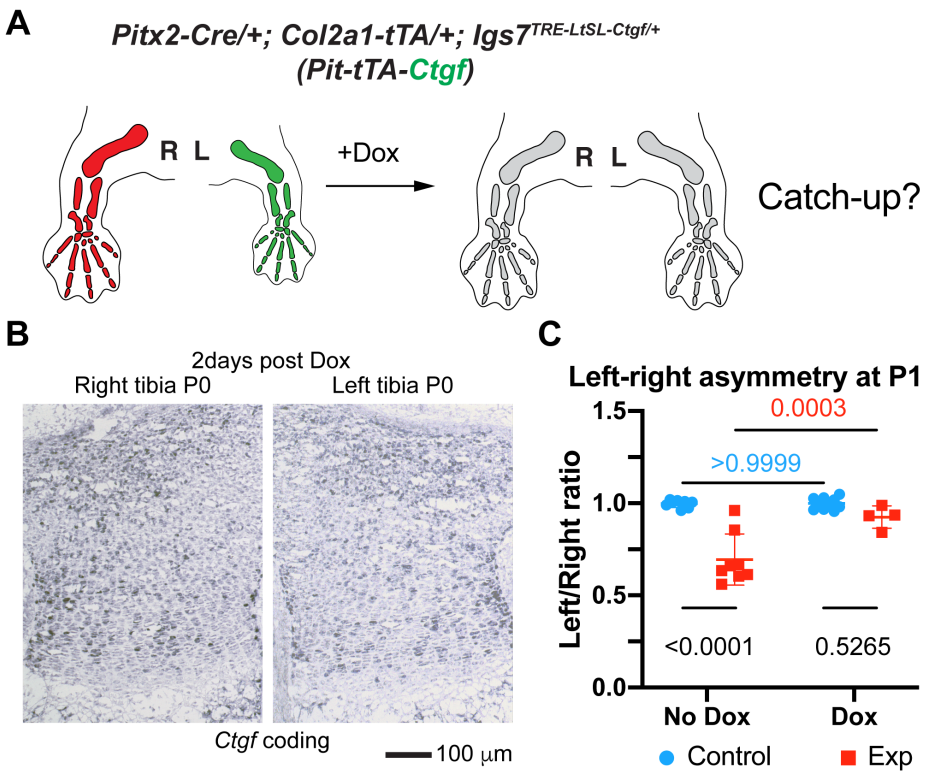

Figure 4. Different outcomes of transient vs. continuous expression of *Ctgf* in the cartilage of the growing bones. A) Schematics of the transient injury experiment. B) Expression of *Ctgf* (coding region) in the proximal cartilage of left and right tibia of *Pit-tTA-Ctgf* P0 pups, 2 days after Dox administration (n=3). C) When transgenic *Ctgf* expression was shut down by Dox treatment in the *Pit-tTA-Ctgf* model (Dox at E17.5, analysis at P0-P1), the asymmetry was not as extreme as in the case of continuous *Ctgf* misexpression (no Dox condition, see schematics). In the graphs, quantification of left/right ratio of bone length is shown for control (tTA^-) and experimental animals (tTA^+), treated or no with Dox. Analysis by 2-way ANOVA for Genotype and Treatment, p-values for Sidak's multiple comparisons post-hoc test are shown. Since we used an internal ratio (left/right length), data from femora and humeri were pooled together. They were treated as independent samples because *Pitx2-Cre* has been shown to recombine with different efficiencies in forelimb and hindlimb (Rosello-Diez et al., 2018).

The *Dragon* lines are effectively activated by (r)tTA and Cre, and not leaky.

We then performed in-depth characterization of the described lines, to make sure they were tightly and efficiently regulated in a variety of scenarios. In previous studies we showed that *TRE*-driven transgenes are highly expressed from the *Tigre* locus when insulator elements and a Woodchuck virus RNA stabilizing sequence are included (Madisen et al., 2015; Rosello-Diez et al., 2018). However, it has not been tested whether the *Tigre-TRE* driven GOIs are highly expressed in the

presence of other *TREs* that could compete for the transcriptional machinery and rtTA. This is important because one possible non-intersectional application of our system is to combine it with an (r)tTA and a TRE-driven Cre to achieve expression of both Cre and the GOI in a tissue during the time (r)tTA is activated. To address this potential competition, we generated mice bearing a *TRE-Cre* (Perl et al., 2002) and our *Col2a1-tTA* allele–which initiates expression in the cartilage at around E12.5 (Rosello-Diez et al., 2018) and the *Dragon-p21* allele (*Col-TCre-p21* model, Fig. 5A,B). We analyzed the mice at postnatal day (P) 0 in the absence of Dox, such that the tTA was active for at least a week before analysis. In *Dragon-p21* mice that did not contain *tTA* nor *TRE-Cre*, no tdTomato or p21 expression was detected in the target tissue (or other tissues), confirming that there is no spontaneous firing of the *Dragon* allele (Fig. 5C left). In the presence of only *tTA*, we mostly detected tdT^+ cells in the cartilage (Fig. 5C middle), of which very few were $p21^+$, revealing there is negligible read-through activity past the STOP cassette (black dots in Fig. 5D). Finally, when both *TRE-Cre* and *tTA* were present along with the *Dragon-p21* allele, we observed a full switch from *Dragon TRE*-driven tdT to p21 expression (Fig. 5C, D). Since no cells expressed only tdT, this result indicates that the two *TRE*-driven alleles are both effectively induced.

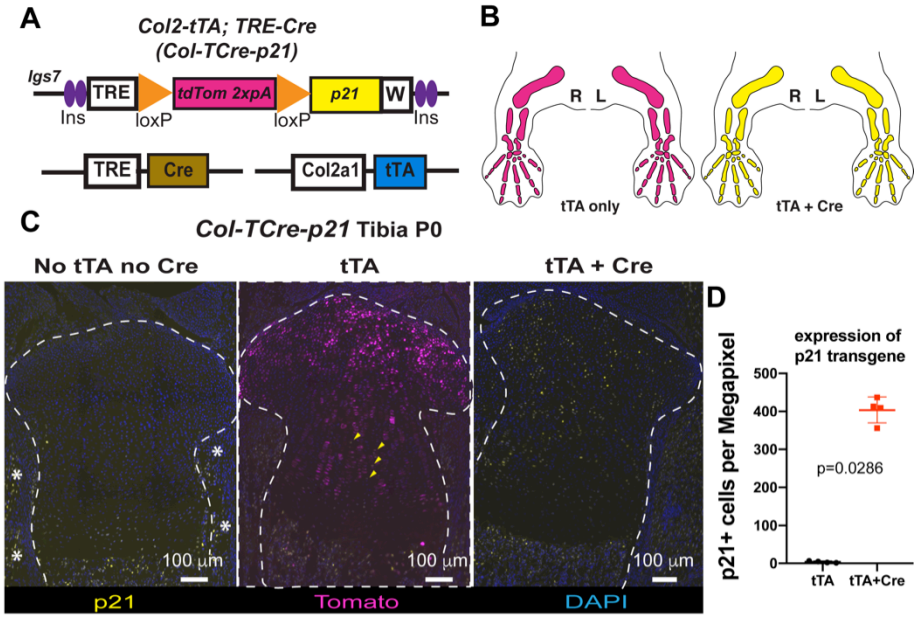

Figure 5. The *Dragon* lines are effectively activated by (r)tTA and Cre, and not leaky. A) Depiction of the alleles that compose a *Col-TCre-p21* model (see text for details). B) Prediction of expression domains [color code as in (A)] in the presence of *Col2a1-tTA* but absence of the Cre allele (left), and when both Cre and tTA alleles are present along with *Dragon-p21* (right). R, L: right and left limbs, respectively. C) Representative micrographs of immunohistochemistry for the indicated proteins on proximal tibia sections from newborn littermates of the indicated genotypes. Dashed lines delimit the cartilage. Arrowheads point to rare tdT^+p21^+ cells indicating read through in the *Dragon-p21* allele. Asterisks indicate endogenous expression of p21 in muscle and perichondrium. D) Quantification of p21 expression in control and experimental mouse sections (n=4 each). p-value for unpaired Mann-Whitney test is shown.

A germline-recombined version of the *Dragon* allele is tightly controlled by (r)tTA only.

To avoid the extra breeding steps required to introduce a third allele such as *TRE-Cre* in non-intersectional applications such as the one described above, we have also generated a germline-recombined version of the *Dragon-p21* allele (*p21rec,* Fig. 6A) that only requires (r)tTA activity to express *p21*. To test this allele, we generated mice containing *Col2a1-rtTA, p21rec* and *Pitx2-Cre* (the latter for control purposes). As expected, when we provided Dox at E12.5, since p21 expression does not require intersection with Cre activity, we observed p21 expression in the same number of chondrocytes in the left and right limbs (Fig. 6B,C). Moreover, a higher percentage of chondrocytes expressed p21 in the limbs (~80%, Fig. 6B,C) than in the left limb of the intersectional approach (50-60% in *Pitx2-Cre/+; Dragon-p21; Col2a1-rtTA* mice, (Rosello-Diez et al., 2018)). This new *p21rec* strain and similar derivatives of our *DTA* and *Ctgf Dragon* alleles will be useful to interfere with cell functions in a variety of contexts, either by using existing tissue-specific (r)tTA mouse lines or Cre-dependent (r)tTAs driven by tissue-specific Cre.

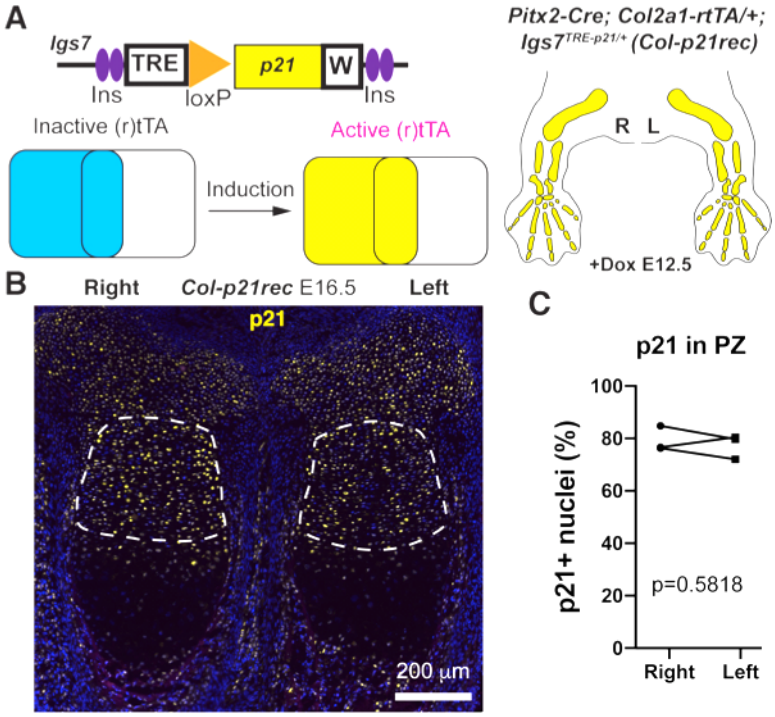

Figure 6. A germline-recombined version of the *Dragon* allele becomes responsive to active (r)tTA only. A) Depiction of the recombined allele (*p21rec*) and how it works in the presence of *Col2-rtTA* (*Col2-p21rec* model). Note that the crosses include *Pitx2-Cre* for control purposes, even though it is not necessary for p21 expression. B) Representative micrograph showing p21 expression in left and right proximal tibial cartilage at E16.5, 4 days after Dox administration. C) Quantification and statistical analysis of $p21^{+}$ cells in the proliferative zone (PZ, delimited by dashed lines). p-value for ratio-paired t-test is shown.

The use of CAG-rtTA3 in combination with *Cre* and *Dragon* lines allows for inducible and reversible transgene expression using a tissue-specific Cre driver, but the level of expression is tissue-dependent.

Given that there are more *Cre* than *(r)tTA* mouse lines available (>700 *Cre* vs. 44 *(r)tTA* lines in JAX), a versatile way to use the *Dragon* mice to achieve conditional reversible induction is to combine our *Dragon* lines with a Cre line that is as tissue-specific as possible and either a Cre-dependent or a constitutively active *rtTA* allele. We tested this approach by combining the *Pitx2-Cre* and *Dragon-p21* alleles with an $R26^{CAG\text{-}rtTA3}$ line that expresses rtTA constitutively (Dow et al., 2014), and providing Dox at E12.5. The expectation was that p21 would be expressed in most of the left limb mesenchyme, and tdTomato everywhere else (Fig. 7A). Surprisingly, however, at P0 the expression levels of both transgenes were very low in the cartilage regions, yet quite high outside the cartilage (Fig. 7B). Given that with another *rtTA* driver and the same *Cre* transgene we previously obtained much higher expression in the cartilage (Rosello-Diez et al., 2018), we conclude that the *CAG-rtTA3* line is not highly expressed in the cartilage. Therefore, we looked at other limb regions, like the interface between cartilage and bone, which is also derived from the *Pitx2-Cre* lineage, and found that the expression levels were higher there, and the number of $p21^{+}$ cells was more abundant in the left limb, as expected (Fig. 7C-D). Hence, while using Cre-activated or constitutive *CAG-rtTA3* in combination with a tissue-specific Cre and our *Dragon* alleles might be an easy way of harnessing the wealth of *Cre* lines available into achieving transgene expression with high spatio-temporal control, our results show that the efficiency of this approach depends heavily on the expression levels of the transgene driving rtTA in the tissue(s) of interest. It remains to be determined if other constitutive *(r)tTA* mouse lines have the same problem, but our own experience and that of our colleagues suggest that the *Rosa26* locus is particularly prone to variegation (Jody Haigh, personal communication).

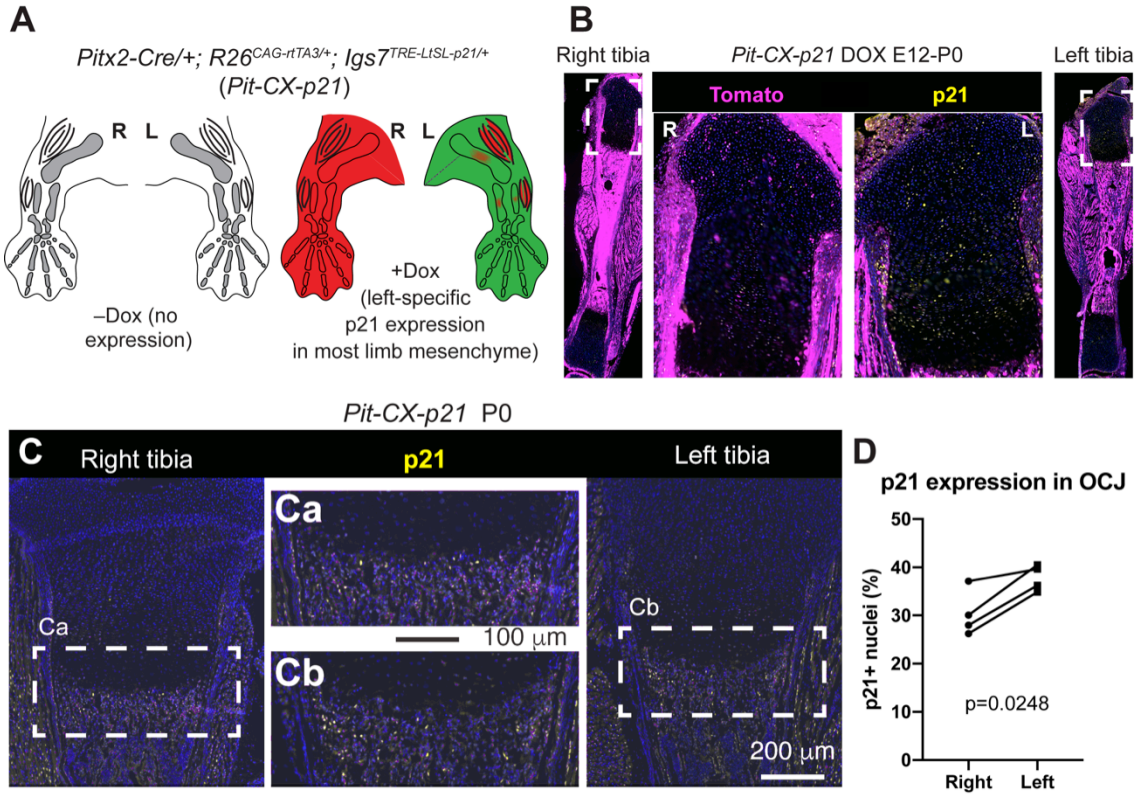

Figure 7. *CAG-rtTA3* in combination with *Cre* and *Dragon* lines allows for reversible transgene expression using tissue-specific *Cre* drivers. A) Depiction of the *Pit-CX-p21* model to achieve expression of p21 (green) in the left limb mesenchyme, and tdTomato (red) everywhere else. B) Representative micrographs of left (L) and right (R) *Pit-CX-p21* tibias (and close-ups of the boxed cartilage regions) at P0, after 1 week Dox treatment. Note the much fainter expression of tdTomato in the cartilage as compared to the surrounding tissues. C) Same as (B), focusing on the osteo-chondral junction (OCJ, limit between the cartilage and bone, magnified in Ca, Cb). D) The number of $p21^{+/-}$ nuclei was quantified in the left and right regions shown in (C, n= 4 pairs of limbs). p-value for ratio-paired t-test is shown.

The *Dragon* targeting vectors can be used for *in ovo* electroporation.

Lastly, we tested the possibility of using the *Dragon* tools in animal models other than the mouse. The chicken embryo has been a classical model for cell and developmental biology, immunology, virology and cancer that is experiencing a revival since the introduction of modern genetic and imaging tools (Kain et al., 2014; Rashidi and Sottile, 2009; Stern, 2005). *In ovo* electroporation enables the introduction of exogenous genetic constructs in multiple locations of the embryo, in order to perform gain- and loss-of-function studies, lineage tracing, live imaging, etc. (Morin et al., 2017; Scaal et al., 2004). Therefore, we electroporated the right half of the neural tube of chicken embryos at Hamilton-Hamburger (HH) stage 14-17 (Hamburger and Hamilton, 1992) with a mix of *pCAGGS-H2B-TagBFP* (to visualize electroporated cells), *pCAGGS-rtTA-IRES-Cre* (to constitutively express rtTA and Cre) and a targeting vector (*Ai62*) bearing a *TRE-loxSTOPlox-tdTomato* cassette (Madisen et al., 2015). 24 h after electroporation, we observed robust and consistent electroporation (blue signal, Fig. 8A) in the right neural tube of most surviving embryos,

as well as strong red signal in the electroporated area of Dox-treated embryos (Fig. 8A). Embryos not treated with Dox did not show any red signal (Fig. 8B). Detailed examination on sections revealed some cases in which all electroporated cells showed tdTomato signal (n=3 embryos out of 11), although it was frequent to observe some cells (~25% per section) with BFP signal but not tdTomato (Fig. 8C, n=8 out of 11 embryos). Assuming all electroporated cells incorporated all vectors, this suggests either that the *CAGGS* promoters in the two plasmids compete for the transcriptional machinery (Christophe Marcelle, personal communication), and/or that the Cre is expressed at suboptimal levels as a consequence of being placed downstream of the IRES sequence (Mizuguchi et al., 2000). Regardless, our results indicate that the plasmids we have generated for mouse ES cell targeting can be directly used for efficient *in ovo* electroporation, opening the door for precise gene manipulation in other animal models. The use of tissue-specific rather than ubiquitous promoters would make the system more versatile in the future. Another advantage of the chicken model is the possibility of combining genetic manipulation with direct physical manipulation. For example, one could co-electroporate vector(s) containing *rtTA* and the *Dragon* construct, induce recombination of the construct in a restricted region of the embryo by placement of beads soaked with cell-permeable Cre (Gitton et al., 2009) and administration of Dox to activate the gene of interest only in the primed region. The possibilities are only limited by the skill and imagination of the operator.

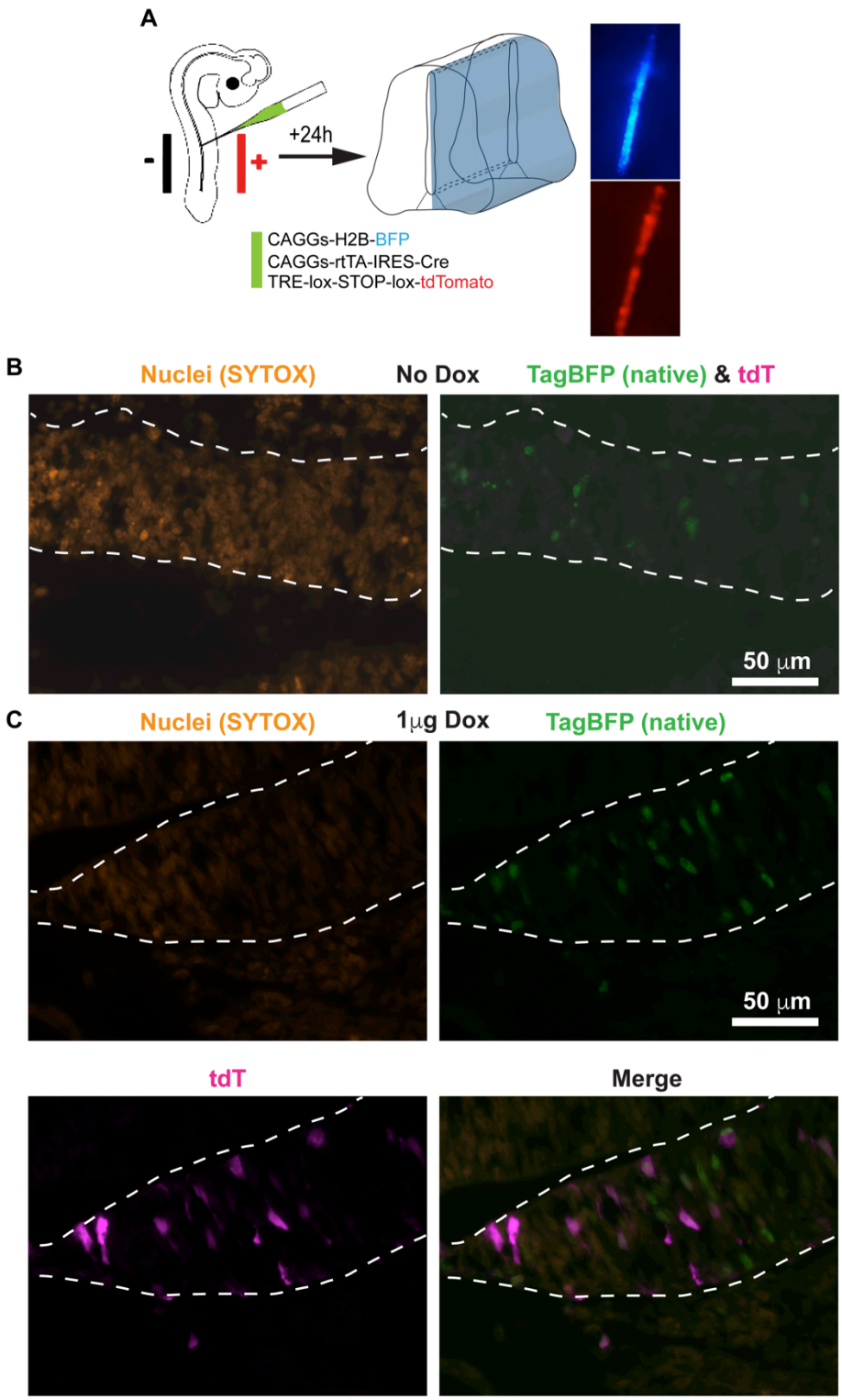

Figure 8. The *Dragon* vectors can be used for *in ovo* electroporation. A) Schematics of the electroporation procedure in the neural tube of chicken embryos (cartoon), and representative examples of the outcome (micrographs taken on a fluorescence dissecting microscope). B-C) Individual and merged channels of transverse neural tube sections (dashed lines) from electroporated chicken embryos, either untreated (B, n=2), or Dox-treated (C, n=11), 24 h after electroporation. In order to be able to visualize the native fluorescence of BFP, we used a green nuclear stain (SYTOX Green).

In summary, we have expanded and further tested the repertoire of *Dragon* intersectional tools and demonstrate their advantages for *in vivo* studies. With the ever-increasing number of *Cre* and *(r)tTA*

mouse lines available, we anticipate that this system will be useful to many researchers across different fields. One potential limitation of these tools is that whereas the constructs also work very well for transfection *in vitro* using HEK cells (not shown), they are probably not suitable for viral transduction, as they tend to be quite big (>10 kb) due to the inclusions of insulators and RNA-stabilizing sequences. All the mouse lines and constructs described here will be submitted to repositories to make them available for the scientific community.

ACKNOWLEDGEMENTS

We thank past and present members of the Joyner and Rosello-Diez laboratories for discussions and technical help. We are grateful to Dr. Miguel Torres for providing a polyclonal antibody to all isoforms of mouse MEIS2. We acknowledge the assistance from Monash Animal Research Platform (MARP), Monash Micro Imaging Platform (MMI) and the Sloan Kettering Institute Research Animal Resource Center and Mouse Genetics Core Facility. Plasmid *pT2-CAGGS-H2B-BFP* was a kind gift of the Marcelle lab. Addgene plasmids #20910 (*PB-CA-rtTA* Adv) and #102423 (*PB-CAGGS-rtTA-IRES-Hygro*) were donated by the Nagy and Koh labs, respectively. This work was supported by grants from the Human Frontiers Science Program (LT000521/2012-L and CDA00021/2019) and Charles Revson Foundation (grant number 15-34) to A.R-D., Monash Graduate Scholarship (MGS), Monash International Tuition Scholarship (MITS) and the Islamic Development Bank (36/115444) funds to E.A., NYSTEM Postdoctoral fellowship to NSB (#C32599GG), NIH to A.L.J. (R21 HD083860 and R01 NS092096) and a National Cancer Institute Cancer Center Support Grant (P30 CA008748-48). The Australian Regenerative Medicine Institute is supported by grants from the State Government of Victoria and the Australian Government.

AUTHOR CONTRIBUTIONS

E.A.: performed some *Dragon-Ctgf* and all chicken experiments and edited the manuscript; A.S.: performed data analysis and edited the manuscript; X.Q.: assisted with genotyping, cloning, embryo dissection and histology; N.S.B.: performed *eCN-DTA* experiments and analysis, D.S. assisted with breeding, genotyping and histology throughout the project; L.M. and H.Z.: performed ES cell targeting and provided key reagents; A.L.J was involved in experimental design, funding acquisition, supervision and manuscript editing; A.R-D. was responsible of conceptualization, funding acquisition, experimental design and procedures, data acquisition and analysis, supervision, manuscript drafting and editing.

DECLARATION OF INTERESTS

There are no conflicts of interest.

STAR ★ METHODS

KEY RESOURCES TABLE

REAGENT or RESOURCE	SOURCE	IDENTIFIER
Antibodies		
rat monoclonal anti-mCherry	ThermoFisher	M11217 mAb; RRID:AB_2536611
rabbit polyclonal anti-p21	Santa Cruz	M19 pAb; RRID:AB_632123
Rabbit polyclonal anti-MEIS2	Mercader et al., 2005	N/A
Anti-Digoxigenin-AP Fab fragments	Sigma-Aldrich	11093274910; RRID:AB_514497
Chemicals, recombinant proteins		
Paraformaldehyde (powder)	Sigma-Aldrich	
Triton X-100	Sigma-Aldrich	T9284-500ML
Fluoromount aqueous mounting medium	Sigma-Aldrich	F4680-25ml
40,6-diamidino-2-phenylindole (DAPI)	ThermoFisher	D1306
SYTOX green	ThermoFisher	S7020
Doxycycline hyclate	Sigma-Aldrich	D9891-10 gr
Biotin 16-dUTP	Sapphire Bioscience	JBS-NU-803-BIO16-S
Terminal transferase recombinant	Merck	3333566001
Electroporation tools		
Platinum wire, 0.25 mm	SDR Scientific	711000
Tungsten wire, 0.5 mm	Sigma-Aldrich	356972
Pulse generator and amplifier	Intracel	TSS20
Glass capillaries	Harvard apparatus	GC120T-10
Experimental Models: Organisms/Strains		
Mouse *Igs7*$^{TRE\text{-}LtSL\text{-}p21}$	Rosello-Diez et al., 2018	N/A
Mouse *Igs7*$^{TRE\text{-}p21}$	This paper	N/A

Mouse *Igs7*$^{TRE\text{-}LtSL\text{-}Ctgf}$	This paper	N/A
Mouse *Igs7*$^{TRE\text{-}LtSL\text{-}DTA}$	This paper	N/A
Mouse B6.Cg-Gt(ROSA)26Sortm1.1(CAG-rtTA3)Slowe/LdowJ	Dow et al., 2014	RRID:IMSR_JAX:029627
Mouse *Col2a1-tTA*	Rosello-Diez et al., 2018	N/A
B6C3(129)-Tg(Pitx2ASE-cre)16Hmd/HmdRbrc Mus musculus	Shiratori et al., 2006	RRID:IMSR_RBRC03487
Tg(Col2a1-rtTA,tetO-COMP)1Jath	Posey et al., 2009	RRID:MGI:4361029
Plasmids		
pPB-CA-rtTA-Adv	Addgene	RRID:Addgene_20910
pPB-CAG-rtTA-IRES-Hygro	Addgene	RRID:Addgene_102423
pT2-CAG-H2B-TagBFP	Sieiro et al., 2016	N/A
pCAGGs-rtTA-IRES-Cre	This paper	AR98
Ai62(TITL-tdT) Flp-in replacement vector	Madisen et al., 2015	RRID:Addgene_61576

LEAD CONTACT AND MATERIALS AVAILABILITY

Further information and requests for resources and reagents should be directed to and will be fulfilled by the Lead Contact, Alberto Rosello-Diez (alberto.rosellodiez@monash.edu).

EXPERIMENTAL MODEL AND SUBJECT DETAILS

Generation and maintenance of mouse lines

The generation of the *Igs7*$^{TRE\text{-}LtSL\text{-}p21}$ (*Dragon-p21*) mouse line was as described (Rosello-Diez et al., 2018). To generate the *Igs7*$^{TRE\text{-}p21}$ mouse line (*p21rec*), *Dragon-p21* males were crossed with germline Cre-expressing females to delete the floxed cassette. The Cre allele was subsequently eliminated during the breeding to generate *p21rec* homozygous animals.

To generate the *Igs7*$^{TRE\text{-}LtSL\text{-}Ctgf}$ mouse line, the *NruI*-STOP-loxP-tdTomato-*SnaBI* fragment in the *Ai62(TITL-tdT) Flp-in* replacement vector (Madisen et al., 2015) was replaced by a custom *NruI-tdTomato-STOP-loxP-MluI-HpaI-SnaBI* cassette, to generate an empty DRAGON vector. A PCR-amplified Kozak-*Ctgf* cassette was subsequently cloned into the *MluI* and *SnaBI* sites to generate the *DRAGON-Ctgf* vector. This vector was then used for recombinase-mediated cassette exchange into *Igs7*-targeted G4 ES cells (Madisen et al., 2015). Two successfully targeted clones (#1 and #2) were injected into C2J blastocysts to generate chimeras, obtaining 11 chimeric males that survived

(out of 30 animals born) with 25-85% chimaerism. One male from clone #1 and three males from clone #2 were crossed to Swiss Webster mice (Charles River) to assess germline transmission. Only clone #2 was successfully transmitted and used to establish the new mouse line.

A similar process was used to generate the *Igs7*$^{TRE\text{-}LtSL\text{-}DTA}$ mouse line, with the only difference being that an attenuated version of DTA (tox176) was used to PCR-amplify the Kozak-DTA cassette. Two successfully targeted clones (#8 and #13) were injected into C2J blastocysts to generate chimeras, obtaining 34 chimeric males that survived (out of 52 animals born) with 35-100% chimaerism. Four males from clone #8 and two from clone #13 were used to assess germline transmission and establish the new mouse line.

All mouse lines were maintained on an outbred Swiss Webster background. The DNA primers and programs used for genotyping each allele and transgene are shown in Table 1:

Allele	**Program**	**Primer name**	**Primer sequence (5' to 3')**
Cre	94ºC 2', 33x(94ºC 20", 60ºC 20", 72ºC 30"), 72ºC 5', 10ºC forever)	Cre F Cre R	GCGGTCTGGCAGTAAAAACTATC GTGAAACAGCATTGCTGTCACTT
Dragon WT	94ºC 2', 33x(94ºC 20", 55ºC 20", 72ºC 30"), 72ºC 5', 10ºC forever)	Dragon F Dragon R WT	CCCAACGGTCACTTACTTCC CACACCTTTAATCCCGATGC
Dragon Mut	94ºC 2', 10x(94ºC 20", 65ºC-0.5/cycle 15", 68ºC 10"), 72ºC 5', 10ºC forever), 28x(94ºC 15", 60ºC 15", 72ºC 10"), 72ºC 2', 10ºC forever)	Dragon F Dragon R Mut	CCCAACGGTCACTTACTTCC GGTAACCGCGGCATAAAAC
p21rec	94ºC 2', 33x(94ºC 20", 55ºC 20", 72ºC 30"), 72ºC 5', 10ºC forever)	Pmin F WPRE Rev	AGTGAACCGTCAGATCGC GCGTATCCACATAGCGTAAAAG

Col2-rtTA	94ºC 2', 33x(94ºC 20", 61ºC 20", 72ºC 30"), 72ºC 5', 10ºC forever),	rtTA F rtTA R	ATGCCCTTGGAATTGACGAGTACGG CGAGGCTTGCAGGATCATAATCAG
Col2-tTA	94ºC 2', 33x(94ºC 20", 55ºC 20", 72ºC 30"), 72ºC 5', 10ºC forever)	Col2a1 F tTA R	CCAGGGTTTCCTTGATGATG GCTACTTGATGCTCCTGATCCTCC
CAG-rtTA3	94ºC 2', 33x(94ºC 20", 55ºC 20", 72ºC 30"), 72ºC 5', 10ºC forever)	Mut F Common Rev WT F	AAAGTCGCTCTGAGTTGTTAT GCGAAGAGTTTGTCCTCAACC GGAGCGGGAGAAATGGATATG

Table 1. Primers and PCR conditions used for genotyping

Animal experiments

All mouse work was carried out according to institutional guidelines after obtaining their approval (Sloan Kettering Institute IACUC and Monash University Animal Ethics Committee). For time-mated crosses, vaginal plugs were checked in the mornings, and noon of the day the plug was detected was considered E0.5. When Dox was needed, it was added to the drinking water. To activate *Col2a1-rtTA*, the final concentration was 1 mg/ml, including 1% sucrose to increase palatability. To inactivate *Col2a1-tTA* and *Atoh1-tTA*, the final concentration of Dox was 0.02 mg/ml.

Upon reception, chicken eggs were kept at 18ºC for up to 2 weeks. Two and half days prior to the experiment, they were transferred to a watered incubator at 37ºC with forced ventilation.

In ovo electroporation

In ovo electroporation was performed as described (Blank et al., 2007). Briefly, on the day of the experiment, eggs were laid out horizontally; 3 ml of albumin were removed from the blunt end of each egg, and a window was opened on top with blunt forceps. A few drops of Ringer's solution containing Penicillin-Streptomycin (Gibco 15140122, diluted 1/50) were pipetted on top, and the membranes removed with a hooked needle. Indian ink (drawing ink A, Pelikan #201665, diluted 1/100 in Ringer's solution) was injected under the vitelline membranes to provide contrast. A pulled glass capillary (Harvard apparatus GC120T-10) and a mouth pipette were used to inject into the caudal neural tube the electroporation mix (1 µg/µl each plasmid in injection solution: high

viscosity carboxymethylcellulose 0.33% (Sigma); Fast Green 1% (Sigma); $MgCl_2$ 1 mM in PBS). Custom-made electrodes (using 0.5-mm wide platinum wire for the positive electrode and a tungsten wire for the negative one) were placed flanking the embryo, and a pulse generator (Intracel TSS20 with current amplifier) used to deliver 3 square pulses (27 V, 30 ms ON, 100 ms OFF). After electroporation, 200 µl of Doxycycline solution (5 ng/µl in Ringer's) were micropipetted underneath the embryo. Eggs were then sealed with tape and incubated for 24h.

METHOD DETAILS

Cloning of pCAGGS-rtTA-IRES-Cre

The vector for constitutive expression of rtTA and Cre was built via Gibson cloning using Addgene #20910 (digested *SmaI-PacI*) as backbone, and the following fragments: an *IRES* sequence amplified from Addgene #102423 using primers CTTGACATGCTCCCCGGGTAACCCCTCTCCCTCCCCCCC and GCTCCATTCATTTATCATCGTGTTTTTCAAAGGAAAACCACG, and a Cre sequence amplified from genomic DNA of a *Cre*$^+$ mouse with primers AAACACGATGATAAATGTCCAATTTACTGACCG and ATGCTCTCGTTAATCTAATCGCCATCTTCCAG. The molecular assembly was done with the NEBuilder HiFi DNA Assembly cloning kit following manufacturer instructions.

Sample collection and processing

Mouse limbs: Upon embryo or pup collection, the limbs were dissected out in cold PBS, skinned and fixed in 4% PFA for 2 days. No decalcification was done for samples P1 or younger. After PBS washes, the limbs were cryoprotected in PBS with 15% sucrose and then equilibrated at 37ºC in PBS with 15% sucrose and 7.5% porcine skin gelatin (Sigma) until they sank. The limbs were oriented inside the wells of multi-welled plates and cooled down until solid, to then flash-freeze them using a dry-ice cold bath of isopentane (Merck). The cryoblocks were sectioned at 7 µm on a cryostat (Leica, CM3050S) onto Superfrost slides.

Mouse brains: The brains of all embryonic stages were dissected in cold PBS and immersion fixed in 4% PFA for 24 hours at 4°C. All postnatal stages were transcardially perfused with PBS followed by 4% PFA, and brains were post-fixed in 4% PFA overnight. Specimens for cryosectioning were placed in 30% sucrose/PBS until they sank, embedded in OCT using cryomoulds (Tissue-Tek), frozen in dry ice cooled isopentane, and sectioned at 14 µm on a cryostat (Leica, CM3050S) onto Superfrost slides.

Chicken embryos: the embryos were scooped out of the egg and dissected in cold PBS. The

electroporated section of the trunk was isolated under the fluorescence scope and then fixed in 4% PFA overnight. After PBS washes, specimens were cryoprotected in 15% sucrose and then 30% sucrose in PBS, until they sank. They were then embedded in OCT using cryomoulds (Tissue-Tek), frozen in dry ice cooled isopentane, and sectioned at 7 µm on a cryostat (Leica, CM3050S) onto Superfrost slides.

Immunohistochemistry and TUNEL staining

Mouse brains: Sections were incubator in PBS for 10 min and then blocked with blocking buffer (5% Bovine Serum Albumin (BSA, Sigma) in PBS with 0.1% Triton X-100). Primary antibodies (MEIS2, 1:3000) in blocking buffer were placed on slides overnight at 4°C, washed in PBS with 0.1% Triton X-100 (PBST) and applied with secondary antibodies (1:500 Alexa Fluor-conjugated secondary antibodies in blocking buffer) for 1 hour at room temperature. Counterstaining was performed using Hoechst 33258 (Invitrogen). The slides were then washed in PBST, then mounted with a coverslip and Fluorogel mounting medium (Electron Microscopy Sciences). TUNEL staining was performed prior to secondary antibody incubation using the Biotin-based in situ cell death detection kit (Roche) and following the manufacturer instructions, including an Avidin-Biotin blocking step (Vector Laboratories).

In situ hybridization

The DIG-labeled RNA probe for *Ctgf* was prepared by *in vitro* transcription of a PCR-amplified template from embryonic day 12.5 cDNA, using the following primers: Fwd: 5'-CAGCTGGGAGAACTGTGTAC-3', Rev(T7): 5'-CGATGTTAATACGACTCACTATAGGGGCTCGCATCATAGTTGGGTC-3'.
Hybridization procedure: the slides were warmed in RNAse-free PBS for 20 min at 37°C, then washed again for 5 min at RT and fixed in 4% PFA solution for 20 min followed by two PBS washes. To increase permeabilization, the slides were placed in PBS with 10 µg/ml protein kinase for 10 min at 37ºC and then washed in normal PBS. Sections were fixed in 4% PFA solution for 5 min, rinsed in PBS and set down in the TEA buffer for 10 min at RT. Hybridization: After rinsing in PBS and water, slides received 600 µl of pre-warmed hybridization buffer and were placed at 65ºC in a humified slide box with formamide 50%, for 90 min. The RNA-probes were then diluted in the hybridization buffer (1µg/ml), denatured at 80º C for 15 min, stabilized on ice for 5 min and placed at 65ºC during prehybridization. Sections received 250 µl diluted probe and were kept at 65º C overnight. Post-hybridization treatment: Once the probes were removed, the slides were placed in post-hybridization buffer I at 65º C for 20 min and this step was repeated with Post-hybridization buffer II. At the end of hybridization, the slides were kept at RT for 5 min, washed with MABT

(0.1 M Maleic acid, 0.15 M NaCl, 0.1% Tween20, pH 7.5) and blocked for 90 min at RT in a humidified slide box with MABT containing 1% blocking reagent (Roche # 11096176001) and 10% goat serum. An AP-conjugated anti-DIG antibody (Sigma, 1:4000 in MABT with 1% blocking reagent and 2% goat serum) was added for 2h at RT. After multiple washes with MABT the sections were washed with AP buffer (0.1M Tris-HCl pH 9.5, 0.1M NaCl, 0.05 M $MgCl_2$, 0.1% Tween20, Levamisole 2mM [Sigma]) 2x5 min each. Staining was developed with BM purple (Roche #11442074001) at 37ºC. After several PBS washes, fixation in 4% PFA and then water wash, sections were counterstained in 0.01% Nuclear Fast Red for 10 min at RT followed by dehydration, clearing in xylene and mounting.

QUANTIFICATION AND STATISTICAL ANALYSIS

Image Analysis and Quantification

The regions of interest were isolated from imaged sections of the multiple models. All the parameters including the brightness, contrast, filters, layers were kept the same for all the images in the same study. Cells positive for the signal of interest were counted manually using ImageJ, after acquisition on an Imager Z1 microscope (Zeiss).

Statistical Analysis

The comparisons were done by an unpaired Mann-Whitney test (1 variable and 2 conditions), or by 2-way ANOVA (2 variables and 2 or more conditions) following a matched (paired) design when possible (indicated when not). When left and right measurements were compared within experimental animals only, ratio-paired t-test was used. All the statistical analyses were done using Prism7 software (Graphpad).

REFERENCES

Blank, M.C., Chizhikov, V., and Millen, K.J. (2007). In ovo electroporations of HH stage 10 chicken embryos. J Vis Exp, 408.

Dow, L.E., Nasr, Z., Saborowski, M., Ebbesen, S.H., Manchado, E., Tasdemir, N., Lee, T., Pelletier, J., and Lowe, S.W. (2014). Conditional reverse tet-transactivator mouse strains for the efficient induction of TRE-regulated transgenes in mice. PLoS One *9*, e95236.

Dymecki, S.M., and Kim, J.C. (2007). Molecular neuroanatomy's "Three Gs": a primer. Neuron *54*, 17-34.

Feil, S., Valtcheva, N., and Feil, R. (2009). Inducible Cre mice. Methods Mol Biol *530*, 343-363.

Gitton, Y., Tibaldi, L., Dupont, E., Levi, G., and Joliot, A. (2009). Efficient CPP-mediated Cre protein delivery to developing and adult CNS tissues. BMC Biotechnol *9*, 40.

Godecke, N., Zha, L., Spencer, S., Behme, S., Riemer, P., Rehli, M., Hauser, H., and Wirth, D. (2017). Controlled re-activation of epigenetically silenced Tet promoter-driven transgene expression by targeted demethylation. Nucleic Acids Res *45*, e147.

Gossen, M., and Bujard, H. (1992). Tight control of gene expression in mammalian cells by tetracycline-responsive promoters. Proc Natl Acad Sci U S A *89*, 5547-5551.

Gossen, M., Freundlieb, S., Bender, G., Muller, G., Hillen, W., and Bujard, H. (1995). Transcriptional activation by tetracyclines in mammalian cells. Science *268*, 1766-1769.
Hamburger, V., and Hamilton, H.L. (1992). A series of normal stages in the development of the chick embryo. 1951. Dev Dyn *195*, 231-272.
Heffner, C.S., Herbert Pratt, C., Babiuk, R.P., Sharma, Y., Rockwood, S.F., Donahue, L.R., Eppig, J.T., and Murray, S.A. (2012). Supporting conditional mouse mutagenesis with a comprehensive cre characterization resource. Nat Commun *3*, 1218.
Hillen, W., and Berens, C. (1994). Mechanisms underlying expression of Tn10 encoded tetracycline resistance. Annu Rev Microbiol *48*, 345-369.
Hirrlinger, J., Scheller, A., Hirrlinger, P.G., Kellert, B., Tang, W., Wehr, M.C., Goebbels, S., Reichenbach, A., Sprengel, R., Rossner, M.J.*, et al.* (2009). Split-cre complementation indicates coincident activity of different genes in vivo. PLoS One *4*, e4286.
Kaczmarczyk, L., and Jackson, W.S. (2015). Astonishing advances in mouse genetic tools for biomedical research. Swiss Med Wkly *145*, w14186.
Kain, K.H., Miller, J.W., Jones-Paris, C.R., Thomason, R.T., Lewis, J.D., Bader, D.M., Barnett, J.V., and Zijlstra, A. (2014). The chick embryo as an expanding experimental model for cancer and cardiovascular research. Dev Dyn *243*, 216-228.
Korecki, A.J., Hickmott, J.W., Lam, S.L., Dreolini, L., Mathelier, A., Baker, O., Kuehne, C., Bonaguro, R.J., Smith, J., Tan, C.V.*, et al.* (2019). Twenty-Seven Tamoxifen-Inducible iCre-Driver Mouse Strains for Eye and Brain, Including Seventeen Carrying a New Inducible-First Constitutive-Ready Allele. Genetics *211*, 1155-1177.
Kronenberg, H.M. (2003). Developmental regulation of the growth plate. Nature *423*, 332-336.
Machold, R., and Fishell, G. (2005). Math1 is expressed in temporally discrete pools of cerebellar rhombic-lip neural progenitors. Neuron *48*, 17-24.
Madisen, L., Garner, A.R., Shimaoka, D., Chuong, A.S., Klapoetke, N.C., Li, L., van der Bourg, A., Niino, Y., Egolf, L., Monetti, C.*, et al.* (2015). Transgenic Mice for Intersectional Targeting of Neural Sensors and Effectors with High Specificity and Performance. Neuron *85*, 942-958.
Matei, V., Pauley, S., Kaing, S., Rowitch, D., Beisel, K.W., Morris, K., Feng, F., Jones, K., Lee, J., and Fritzsch, B. (2005). Smaller inner ear sensory epithelia in Neurog 1 null mice are related to earlier hair cell cycle exit. Dev Dyn *234*, 633-650.
Mizuguchi, H., Xu, Z., Ishii-Watabe, A., Uchida, E., and Hayakawa, T. (2000). IRES-dependent second gene expression is significantly lower than cap-dependent first gene expression in a bicistronic vector. Mol Ther *1*, 376-382.
Morin, V., Veron, N., and Marcelle, C. (2017). CRISPR/Cas9 in the Chicken Embryo. Methods Mol Biol *1650*, 113-123.
Perl, A.K., Wert, S.E., Nagy, A., Lobe, C.G., and Whitsett, J.A. (2002). Early restriction of peripheral and proximal cell lineages during formation of the lung. Proc Natl Acad Sci U S A *99*, 10482-10487.
Posey, K.L., Veerisetty, A.C., Liu, P., Wang, H.R., Poindexter, B.J., Bick, R., Alcorn, J.L., and Hecht, J.T. (2009). An inducible cartilage oligomeric matrix protein mouse model recapitulates human pseudoachondroplasia phenotype. Am J Pathol *175*, 1555-1563.
Rashidi, H., and Sottile, V. (2009). The chick embryo: hatching a model for contemporary biomedical research. Bioessays *31*, 459-465.
Rosello-Diez, A., and Joyner, A.L. (2015). Regulation of Long Bone Growth in Vertebrates; It Is Time to Catch Up. Endocr Rev *36*, 646-680.
Rosello-Diez, A., Madisen, L., Bastide, S., Zeng, H., and Joyner, A.L. (2018). Cell-nonautonomous local and systemic responses to cell arrest enable long-bone catch-up growth in developing mice. PLoS Biol *16*, e2005086.
Rosen, B., Schick, J., and Wurst, W. (2015). Beyond knockouts: the International Knockout Mouse Consortium delivers modular and evolving tools for investigating mammalian genes. Mamm Genome *26*, 456-466.

Scaal, M., Gros, J., Lesbros, C., and Marcelle, C. (2004). In ovo electroporation of avian somites. Dev Dyn *229*, 643-650.
Shiratori, H., Yashiro, K., Shen, M.M., and Hamada, H. (2006). Conserved regulation and role of Pitx2 in situs-specific morphogenesis of visceral organs. Development *133*, 3015-3025.
Smedley, D., Salimova, E., and Rosenthal, N. (2011). Cre recombinase resources for conditional mouse mutagenesis. Methods *53*, 411-416.
St-Onge, L., Furth, P.A., and Gruss, P. (1996). Temporal control of the Cre recombinase in transgenic mice by a tetracycline responsive promoter. Nucleic Acids Res *24*, 3875-3877.
Stern, C.D. (2005). The chick; a great model system becomes even greater. Dev Cell *8*, 9-17.
Takigawa, M. (2013). CCN2: a master regulator of the genesis of bone and cartilage. J Cell Commun Signal *7*, 191-201.
Urlinger, S., Baron, U., Thellmann, M., Hasan, M.T., Bujard, H., and Hillen, W. (2000). Exploring the sequence space for tetracycline-dependent transcriptional activators: novel mutations yield expanded range and sensitivity. Proc Natl Acad Sci U S A *97*, 7963-7968.
Zeng, H., Horie, K., Madisen, L., Pavlova, M.N., Gragerova, G., Rohde, A.D., Schimpf, B.A., Liang, Y., Ojala, E., Kramer, F.*, et al.* (2008). An inducible and reversible mouse genetic rescue system. PLoS Genet *4*, e1000069.